Heat Mass Transfer (2011) 47:13–25
DOI 10.1007/s00231-010-0667-6

ORIGINAL

Simulation of boiling heat transfer in small heaters by a coupled cellular and geometrical automata

C. Marcel · F. Bonetto · A. Clausse

Received: 4 September 2009 / Accepted: 16 August 2010 / Published online: 2 September 2010

Abstract Automata are entities defined by mathematical states that change following iterative rules representing neighborhood interactions. A model of automata for pool boiling heat transfer simulation consisting in collections of virtual spheres that change their volumes and move around a certain environment is presented. The approach is an alternative technique to describe the turbulent features of boiling phenomena, such as interfacial topological transitions and fluid-wall interaction. The novel computer model presented here is able to capture the essential features underlying boiling heat transfer and crisis above a small heater, showing good agreement with experimental data reported in the open literature.

List of symbols

A_l	Fraction of area in direct contact with the liquid
c_{mc}	Microconvection constant
g	Gravity acceleration
H	Convection heat transfer coefficient
h_{fg}	Latent heat of evaporation
Ja	Jakob number
k_l	Liquid conduction heat coefficient
k_m	Metal conduction heat coefficient
L	Characteristic cell length
L_c	Channel length
Nu	Nusselt number
p	Breakup probability per time unit
P	Cell perimeter
p_b	Breakup coefficient ($0 < p_b < 1$)
Pr	Prandtl number
$\dot{q}$	Volumetric heat source
q_c	Convection associated heat
q_{mc}	Microconvection associated heat
q_{ml}	Microlayer theory associated heat
r	Bubble radius
r_0	Previous bubble radius
Ra	Rayleigh number
r_c	Critical bubble radius
R_{cav}	Cavity radius
r_d	Detachment bubble radius
t	Time
T	Cellular automata temperature
T_{sat}	Saturation temperature
T_w	Wall temperature
α_l	Liquid thermal diffusivity
β	Volumetric thermal expansion coefficient
Δ	Cell side
Δt	Time that went since the last bubble detachment
ε	Heater emissivity
ϕ	Contact angle
ν	Liquid kinematic viscosity
σ	Surface tension coefficient
σ_{rad}	Stefan–Boltzmann constant
ρ_l	Liquid density
ρ_v	Vapor density
τ	Time lag associated to each change

C. Marcel (✉) · F. Bonetto · A. Clausse
Centro Atómico Bariloche, Av. Bustillo 9500 S.C. de Bariloche, CP 8400 Rio Negro, Argentina
e-mail: christian.marcel@cab.cnea.gov.ar

A. Clausse
Universidad Nacional del Centro, 7000 Tandil, Argentina

1 Introduction

Despite large efforts in the field, the theoretical understanding of boiling processes is still an open area for

research, many questions still remaining unanswered. During the past decades, a large number of experimental and theoretical studies on boiling were addressed in order to clarify this issue. Many of these studies were focused on single bubble or bubble ensemble configurations as well as on models employing a more generalized approach for the prediction of nucleate boiling and/or critical heat flux (CHF).

Due to difficulties found to describe this phenomenon, boiling flows are usually characterized by means of macroscopic averages of local magnitudes, representing the relative amount of each fluid component, the number of bubbles per unit volume, the interfacial area density, the average bubble size, etc. In such representations, bubbly environments are described with partial differential equations in terms of the average fields representing the physical variables. The already classical formulations are the homogeneous equilibrium, the drift-flux, and the two-fluid models [1–3]. Other similar problems of practical importance, such as granular media, in which the topology of the base manifold changes as the system evolves, also present a tough challenge to standard analysis methods. In these systems the passage to the infinitesimal limit (while preserving the internal structure by means of constitutive laws) is justified, but the concomitant loss of detail is seldom recovered in terms of numerical simplicity; one intractable problem having been translated imperfectly into another, almost as intractable as the first one.

In the fifties Ulam and von Neumann [4] conceived the idea of an ingenious mathematical toy called cellular automata. Foreseeing the advent of the computer age, they realized that complex phenomena might be simulated as assemblies of finite cells, which interact according to a small number of simple rules based on heuristic considerations. The interaction rules, generally applied to the immediate neighbors, may or may not bear a resemblance to the actual physical laws governing the phenomena at hand. For fluids, however, it was found that statistical averages tend to the solution of the partial differential equations known to govern the situation—typically, the Navier–Stokes equation [5]. More recently, numerical simulations have shown that complex systems amenable to representation by cellular automata, exhibit certain regularities in their global behavior, thus rising hope that quantitative laws might be formulated to encompass disparate phenomena as earthquakes, stock markets, weather, biological systems, etc. [6–8].

With the spreading of the software agent paradigm [9] as a byproduct of the object orientation programming [10], new tools to tackle collective phenomena became available to the simulation community. Complex processes can be simulated as an assembly of software autonomous entities that interact according to simple rules based on heuristic considerations [11]. Some authors have proposed the use of a hybrid model based on cellular automata integrated with a conventional CFD code in which they define a regular (2D) hexagon lattice (used for the cellular automata part of the algorithm) superimposed to a regular square mesh (used for the CFD part of the model). Such an approach was used to numerically simulate pool boiling with certain degree of success by means of a two-dimensional cellular automata representing the fluid (liquid or vapor) layer adjacent to the heater wall [12]. Recently, Gupta and Ghoshdastidar [52] proposed a three-dimensional coupled map lattice model of pool boiling, which is able to predict the CHF of saturated pool boiling of water. The boiling field was represented by a temperature field defined on a regular spatial grid with periodic boundary conditions. The system dynamics is governed by discrete time rules derived from conservation equations. Nucleation in cavities, thermal diffusion, bubble rising and convection, phase change, and Taylor instability, are calculated from the temperature field.

In this article we show a novel perspective in the modeling of boiling environments, based on virtual bubbly worlds created using geometrical automata, with which one can calculate the flow variables by tracking the bubble stock, book-keeping coalescences, breakups, evaporations and condensations. The model is more general than the classical cellular automata in two respects: (1) in order to describe the bubbles, the grid of cellular automata is dismissed in favor of a trajectory generator (i.e. continuous space), and (2) the rules of interaction involve parameters representing the most relevant variables governing the actual physical interactions between phases. Thus, while retaining the basic philosophy underlying cellular automata, a more realistic model is obtained, offering a useful tool for the modeling of boiling flows.

2 The bubble automata

An automaton is an object defined by states that change following iterative rules. A system of automata is a set of these objects located in a spatial environment that defines individual neighborhoods around each automaton. The rules in such systems represent the interaction of each automaton with its neighborhood. Automata systems exhibit interesting regularities and patterns in their global behavior, providing a useful tool for modeling collective processes. Virtual worlds of interacting entities can be used to represent real complex problems such as fluids, condense matter, species populations, market economy, diffusion of diseases, which ultimately share the concept of complex systems.

The formal definition of an automata system requires the specification of the following aspects:

- *Set of entities* collection of autonomous entities that can perform different tasks, perceiving and reacting to external stimuli, with the number of individuals fixed or varying with time.
- *Neighborhood* subset of entities that affect the state of each individual of the system. In case of an environment associated with a spatial frame of reference, it is customary to define neighborhoods as functions of the distance between individual positions.
- *States* mathematical description of the automaton. The simplest case corresponds to binary automata that can take only two possible values, like a spin lattice.
- *Local transition rule* algorithm that defines the system dynamics in terms of the states of neighbor individuals. The rules can be deterministic or probabilistic. Elements obeying the same rule are said to form a class.

Let us model a bubbly environment by introducing the computer at the starting point of the description, simulating the fluid particles as an automata set. Afterwards statistical averages will be calculated in order to identify the general laws resembling a real flow. The flow of bubbles is represented as a virtual world composed of a continuous liquid container (which can be partitioned in slices to construct arbitrary geometries) and a disperse phase consisting of numerous bubbles (automata) embedded in the liquid. Each bubble is codified as an automaton represented by a sphere. The state of such automaton is simply determined by four scalars corresponding to the radius, r, and the position of the center (x, y, z). One can now imagine a field of spheres (each one associated with its four-scalar state) wandering within a box, resembling bubbles in a liquid environment. To study the statistical properties of this elementary system, let us assume the following set of rules for the automata (which apply iteratively to the whole set of spheres):

a. *Displacement* (Fig. 1a) the center of each sphere is displaced a constant distance in a random direction, to simulate turbulence.
b. *Coalescence* (Fig. 1b) when two or more bubbles collide, they coalesce giving birth to a new bubble conserving the total volume and center of mass. This rule is in accordance with observations reported in literature (e.g. see Figure 17 from [13]).
c. *Breakup* (Fig. 1c) each bubble is allowed to breakup into two bubbles conserving the total volume, with a probability per time unit given by:

$$p = p_b \frac{r^2}{r^2 + r_c^2} \tag{1}$$

where r is the bubble radius, r_c is the critical radius, and p_b is the breakup coefficient ($0 < p_b < 1$).

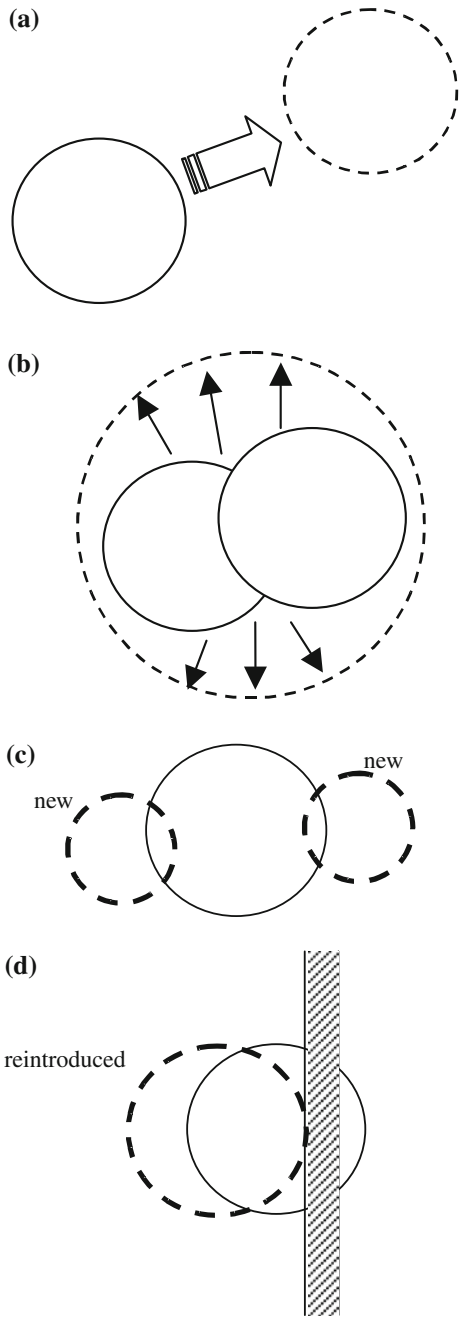

Fig. 1 Basic rules of the bubble automata. **a** Displacement, **b** coalescence, **c** breakup, **d** confinement

d. *Confinement* (Fig. 1d) any bubble moving out of the tube environment through a lateral wall is reintroduced attached to the border.

The model was coded in C language following the object-oriented paradigm [14]. A suitable framework was created to allocate the data for managing the geometrical automata. Details of the implementation of the model can be found in a foregoing section.

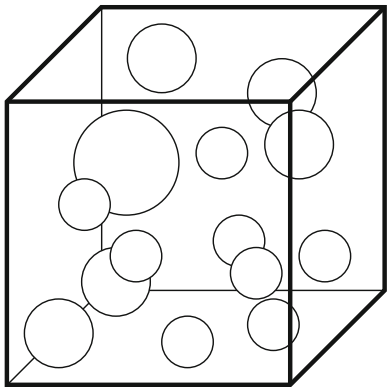

Fig. 2 Bubbles in a box

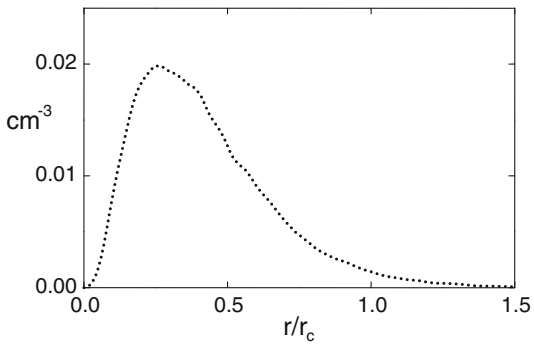

Fig. 3 Equilibrium bubble size distribution in a stirring box (the critical radius is 3% of the box side and the breakup coefficient is 0.7)

The statistical properties of the geometrical automata were studied in a simple case consisting of a certain amount of gas trapped inside a stirring liquid cube (Fig. 2). Fixing the void fraction, the automata were allowed to evolve according to the basic rules. The bubbles randomly move, clash, coalesce and breakup; and one expects to asymptotically find an equilibrium state when the balance of annihilation by coalescence and creation by breakup is reached. Figure 3 shows the equilibrium distribution when the critical radius is 3% of the box side, and the breakup coefficient is 0.7.

3 Pool boiling automata

Pool boiling physics has been extensively studied since the pioneer work of Leidenfrost [15]. The first complete boiling curve was obtained by Nukiyama [16] and very soon researchers realized the importance of the boiling heat transfer crisis. Consequently, great efforts have been devoted to measure and model the boiling process in the past several decades. In their pioneer work, Forster and Zuber [17] presented the bubble agitation model in which the large heat transfer rates associated with nucleate boiling is considered as the consequence of the micro-convection in the superheated sublayer caused by bubble agitation. Moreover, the growth and collapse of vapor bubbles help to remove this sublayer of high thermal resistance. Forster and Greif [18] proposed the vapor–liquid exchange mechanism, that is, the pulsating bubbles draw liquid from the bulk to the heating surface, pushing the heated liquid back into the bulk. Similarly, Han and Griffith [19] put forward the bulk convection theory, considered the departing bubbles bringing part of the layer of superheated liquid adjoining the bubble into the main body of fluid like a small pump. At the same time, cold fluid flows onto the heating surface. By this kind of repeated bulk convection, heat is transferred from the heating surface to the fluid. It is usual to partition the heating surface in pool boiling into two parts: the bulk convection area and the natural convection area. Mikic and Rohsenow [20] extended the bulk convection theory including the effect of the cavity size distribution over the surface. Snyder [21] suggested a microlayer evaporation model in which heat is transferred by the evaporation of a microlayer located under growing vapor bubbles, as well as the condensation of vapor at the top of the bubbles where the vapor bubbles are contacted with relatively colder liquid.

The boiling crisis was always treated as a phenomenon independent of the nucleate boiling process, and almost nothing is known about their interrelation. Some authors have proposed different models which intent to explain the CHF in pool boiling [22–29], including non-linear dynamics [30]. However, to the present it is not clear if one or a combination of these mechanisms determine the occurrence of boiling crisis. Indeed, although great progress has been achieved in this field, the comprehension of the processes involved in boiling heat transfer and crisis is still today one of the most challenging problems in heat transfer technology.

We shall show here how the most important features of pool-boiling heat transfer can be numerically simulated using automata. Let us consider a simple pool boiling scenario consisting of a square-section channel, 4-cm side, 20-cm height, filled with stagnant water at atmospheric pressure. At the channel base there is a copper 1-cm thick plate, dissipating constant heat power, uniformly generated over its volume (see Fig. 4). The heater is isolated in all its boundaries except at the top, therefore forcing the heat flux into the water.

A grid of cubic cellular automata as shown in Fig. 5 represents the heater plate. Each cell is provided with a nucleation site. The size of the cavities is randomly

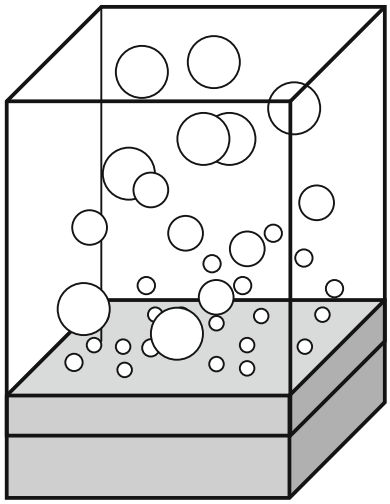

Fig. 4 Pool boiling automata

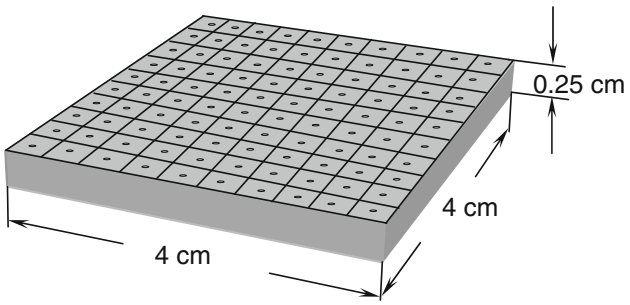

Fig. 5 Diagram of the heater cellular automata

distributed according to a normal distribution (6.1-μm average and 2.4-μm standard deviation). When a site is active, a bubble grows attached to the cell until a critical detachment radius is reached, starting the growth process again with a second bubble, and so on. The detached bubbles are treated as a set of bubble automata that follow the basic rules described before.

A given site nucleates bubbles if its radius, R_{cav}, is in the range [31],

$$\frac{k}{4H}\left(1-\sqrt{1-4\left(\frac{2\sigma HT_{\text{sat}}}{\rho_l h_{fg} k}\right)\frac{1}{T_p-T_{\text{sat}}}}\right)<R_{\text{cav}} < \frac{k}{4H}\left(1+\sqrt{1-4\left(\frac{2\sigma HT_{\text{sat}}}{\rho_l h_{fg} k}\right)\frac{1}{T_p-T_{\text{sat}}}}\right) \quad (2)$$

where H is the convection heat transfer coefficient, T_{sat} is the saturation temperature, T_p is the wall temperature, ρ_l is the liquid density, h_{fg} is the latent heat of evaporation, σ the surface tension and k is the liquid thermal conductivity. The convection heat transfer coefficient is calculated using the average temperature of the heat transfer surface.

The growth of the attached bubble is described by Cooper [32], Cooper and Lloyd [33, 34] and Cooper and Vijuk [35]

$$r(\Delta t) = 2.26 Pr^{-1/2} Ja(\alpha_l \Delta t)^{1/2} \quad (3)$$

being Δt the time lag since the previous bubble detachment, Pr the Prandtl number and Ja the Jackob number which is defined as $Ja = c_p(T_p - T_{\text{sat}})/h_{fg}$ with T_p being the temperature of the nucleating cell. Equation 3 is valid until the bubble radius reaches the Fritz detachment radius r_d expressed as [36],

$$r_d = 0.0104\phi\sqrt{\frac{\sigma}{g(\rho_l-\rho_g)}} \quad (4)$$

where ϕ and g are the contact angle and the gravity.

4 Heater cellular automata

A single positive real scalar variable, T, is assigned to each heater cell, representing the local temperature of the metal. The temperature field in the heater is governed by the Fourier equation, which is discretized applying an upwind scheme, leading to the following rule of the heater cellular automata:

$$T_{xyz}(t+\tau) = T_{xyz}(t) + Fo\left(\sum_n T_n(t) - 6T_{xyz}(t) + \frac{\dot{q}}{k_m}\Delta\right) \quad (5)$$

where the summation is performed over the cells neighboring (x, y, z), t is the time, Fo the Fourier number $Fo = \frac{\alpha\tau}{\Delta^2}$, τ the time step, Δ the cell side, and k_m the heater thermal conductivity.

In order to assure the numerical stability of the explicit finite difference heat conduction equation, the time step in the simulations is chosen so the Fourier number is <1/6.

To simulate the heat extraction from the cells, four different mechanisms are considered: natural convection q_c, microlayer evaporation q_{ml}, microconvection q_{mc} and radiation q_{rad}. The total cellular heat source, $\dot{q}$, results from the summation of the power generated inside the cell minus the heat extracted through the top given by the aforementioned mechanisms. Bubbles close to the surface are allowed to intersect the metal, and the fraction of the cell surface covered by a bubble is considered isolated. Natural convection heat transfer and microlayer evaporation are proportional to the fraction of the cell surface in contact with the liquid, A_l (see Fig. 6). A_l is determined by subtracting the portion of the cell covered by a bubble to the total cell area. The natural convection heat transfer rate q_c

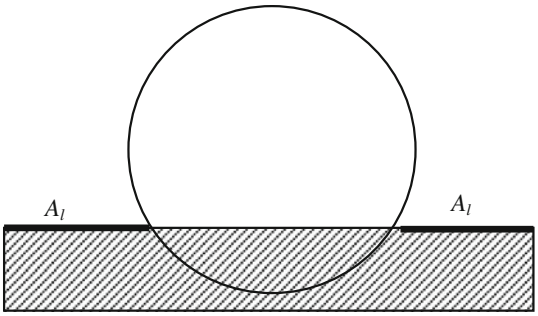

Fig. 6 Fraction of cell surface in direct contact with the liquid

is given by McAdams [37], Goldstein et al. [38] and Lloyd and Moran [39]

$$q_c = \frac{A_l k_l}{L} Nu(T_s - T_l) \tag{6}$$

with the characteristic length L is given by

$$L = \frac{A_l}{P}, \tag{7}$$

the Nusselt number by:

$$\begin{aligned} Nu &= 0.54 Ra^{1/4} \quad \text{if } 10^4 \le Ra_L \le 10^7 \\ Nu &= 0.15 Ra^{1/4} \quad \text{if } 10^7 \le Ra_L \le 10^{11}, \end{aligned} \tag{8}$$

and the Rayleigh number by:

$$Ra = \frac{g\beta(T_s - T_\infty)L^3}{\nu\alpha_l} \tag{9}$$

β being the thermal expansion coefficient of the liquid.

The microlayer term is considered to be proportional to the bubble growth according to the Snyder model [40]. The heat extracted during the evaporation of the microlayer q_{ml} is therefore given by

$$q_{\mathrm{ml}} = \frac{4}{3}\pi\left[r^3(\Delta t) - r_0^3\right]\rho_g h_{fg} \tag{10}$$

where Δt is the time lag since the last bubble detachment.

Microconvection acts when the bubble leaves the surface, extracting a fixed amount of heat proportional to the detaching-bubble volume. The heat removed by microconvection is estimated as [41]

$$q_{\mathrm{mc}} = c_{\mathrm{mc}} r_d^3 \rho_l C_P \Delta T \tag{11}$$

where c_{mc} is a constant coefficient representing the liquid volume around the bubble.

The heat extracted by means of radiation is calculated as [42]

$$q_{\mathrm{rad}} = A\varepsilon\sigma_{\mathrm{rad}}(T_s^4 - T_l^4) \tag{12}$$

with A being the cell area, ε the heater emissivity and σ_{rad} the Stefan–Boltzmann constant.

5 Computational implementation of the model

The data organization for the geometrical automata includes a structure consisting of five different variables. These variables correspond to the radius, the three spatial coordinates and a value indicating the automata state (which accounts for the type of bubble, i.e. spherical or film type).

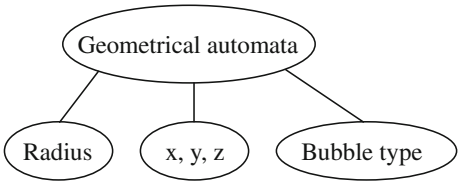

Two different types of data structures are used for implementing the cellular automata simulating the heater. A structure with four different values is needed for describing the heater inner cells. These correspond to the three indexes determining the position and one more for the cell temperature. In the structure used for the cellular automata describing the cells adjacent to the coolant, however, three more values are needed. These extra values correspond to the size of the nucleation cavity, an index indicating whether such a cavity is active or not, and a variable for accounting the size of the growing bubble.

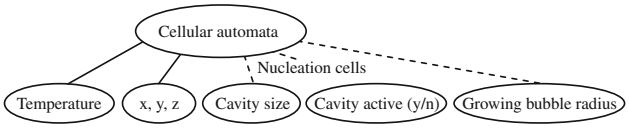

A strong feature of automata implementation is the reduced computer costs needed to simulate a large number of bubbles. For instance, in the simulations reported here the vector used to represent the bubbles with the aforementioned structure had a length of 1,000 automata. As a result of the simplicity of the model and the reduced computer costs, the simulations reported in this work lasted $<$20 h in a normal PC with 1 Gb RAM.

6 Results

Boiling simulations of 60 s total duration and 0.8 ms time step were performed at different heat power levels. In the image sequence shown in Fig. 7, the temperature of the heater surface after a heat power of 0.3 W/cm^2 is suddenly switched on, is depicted. A remarkable characteristic is the time scale: the time required for the creation and detachment of a bubble is about 0.6 s. At the beginning, there are two active sites forming two bubbles. One of these cavities

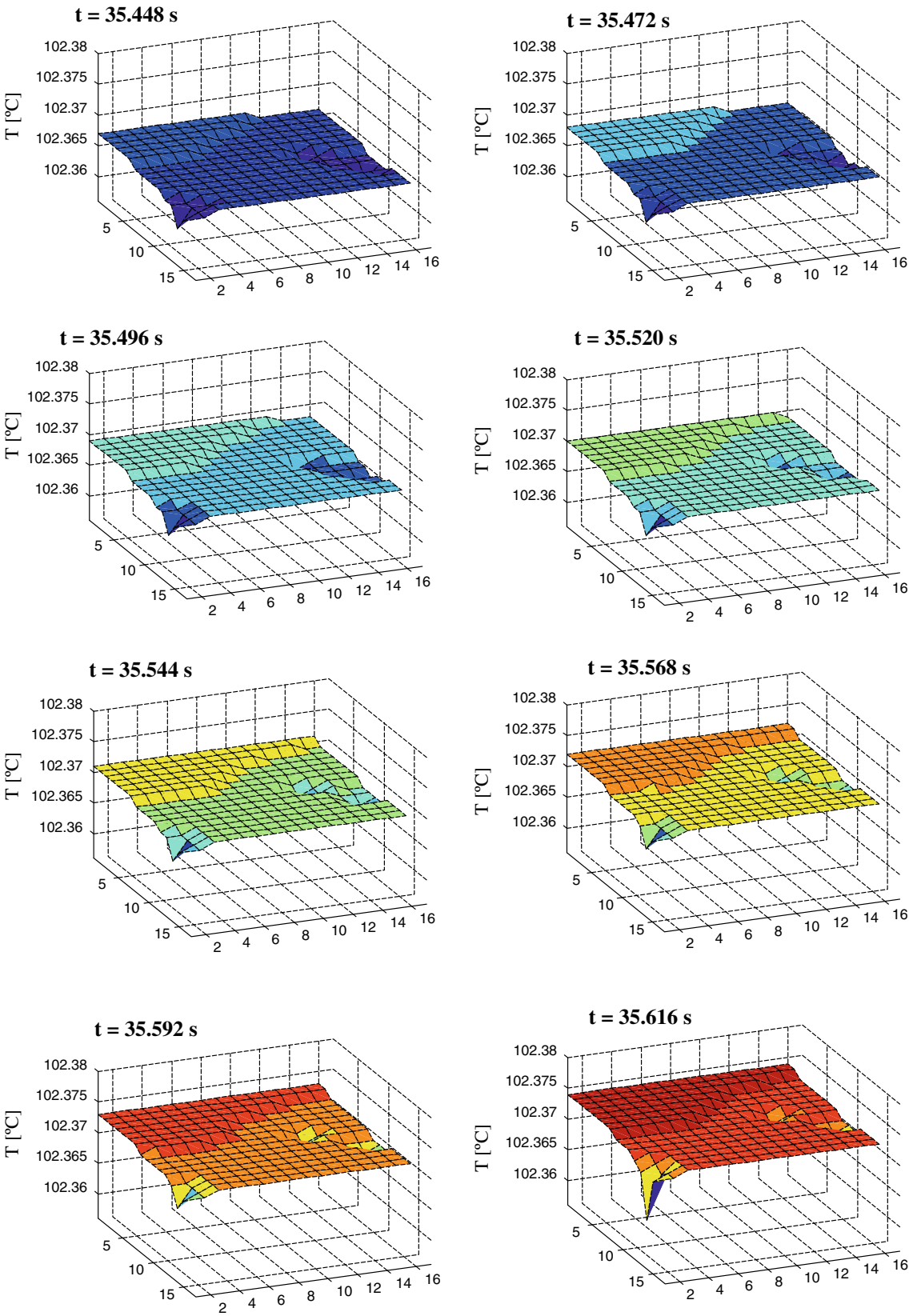

Fig. 7 Sequence of the temperature map of the heater surface after the heat power is suddenly switched on

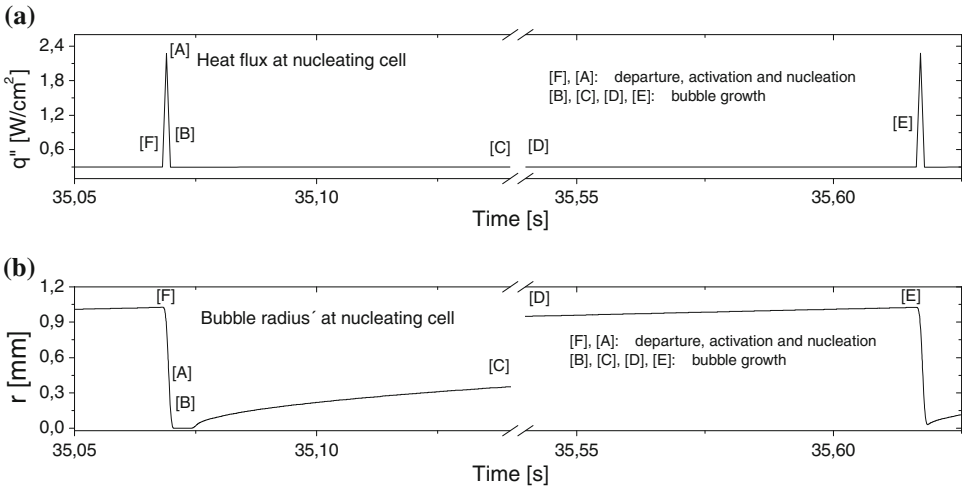

Fig. 8 **a** Time evolution of the heat flux in the nucleating cell associated with the bubble departing at ∼35.6 s. **b** Time evolution of the radii of the departing bubble

has a bubble that detaches at $t \sim 35.6$ s, which produce a sharp decrease in the associated cell temperature and its neighborhood. This behavior is also observed in the experiments reported in [43]. The site looses its activity during a short period, but rapidly the cell temperature rises activating the site again, and a new bubble starts to grow. As time goes on, the temperature of the whole system rises.

Bubble nucleation affects not only the associated sites but also the neighbors. This influence can interfere and even deactivate sites placed a couple of centimeters away from the active site (the cell side is 2.5 mm). This long-range influence is caused by the high thermal conductivity of the copper, and it is much more important at higher powers, for which more sites are active.

Figure 8a shows the time evolution of the heat flux removed in the nucleating cell corresponding to the bubble detaching at ∼35.6 s. The large peak shown in the figure corresponds to the microconvection effect acting at the bubble departure. Interestingly, the general trend shown in Fig. 8 is in excellent agreement to the experimental findings reported in [44]. Agreement is also found when comparing the results with [45] for which the appropriate scaling rule is applied [46]. These results confirm that the main phenomena relevant to the heat transfer and the bubble formation process are well captured by the model. Figure 8b shows the time evolution of the radii of the same bubble during the growing process. Note the small time lag associated with the reactivation of the nucleation site right before the bubble birth.

In Figs. 9 and 10, main characteristics of the flow pattern obtained at a power level of 10 W/cm^2 are presented. Figure 9 shows the histogram of bubble radii constructed by counting and classifying the bubbles. As can be clearly seen, the bubbly flow pattern is characterized by a small number of interactions between the bubbles: the position of the largest peak corresponds to the detaching radii. The void fraction across the heater center, averaged along the axial direction, is depicted in Fig. 10. It can be seen that the model recover wall peak characteristic found in several experiments on two-phase flow channels [47–49].

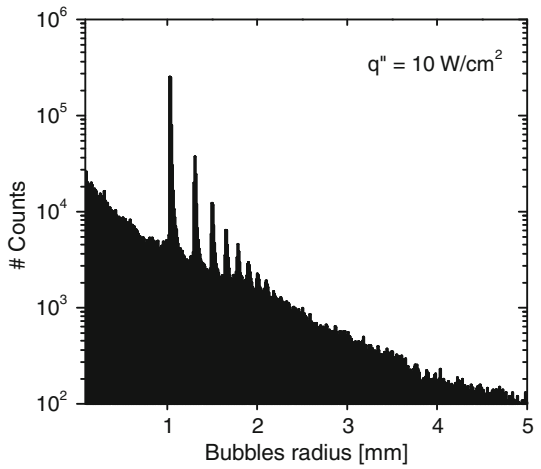

Fig. 9 Histogram of bubble radii in the square channel. The largest peak corresponds to the detaching radii

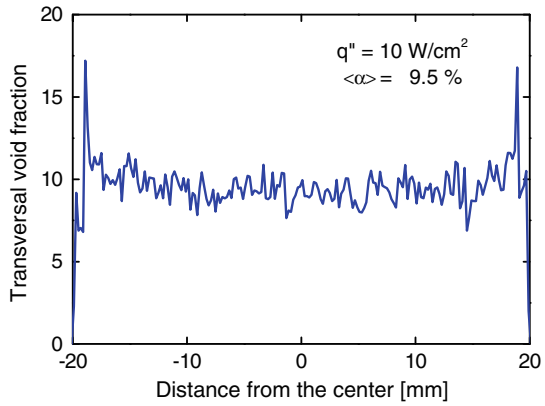

Fig. 10 Averaged center line void fraction distribution. The average void fraction is 0.95 (10 W/cm^2)

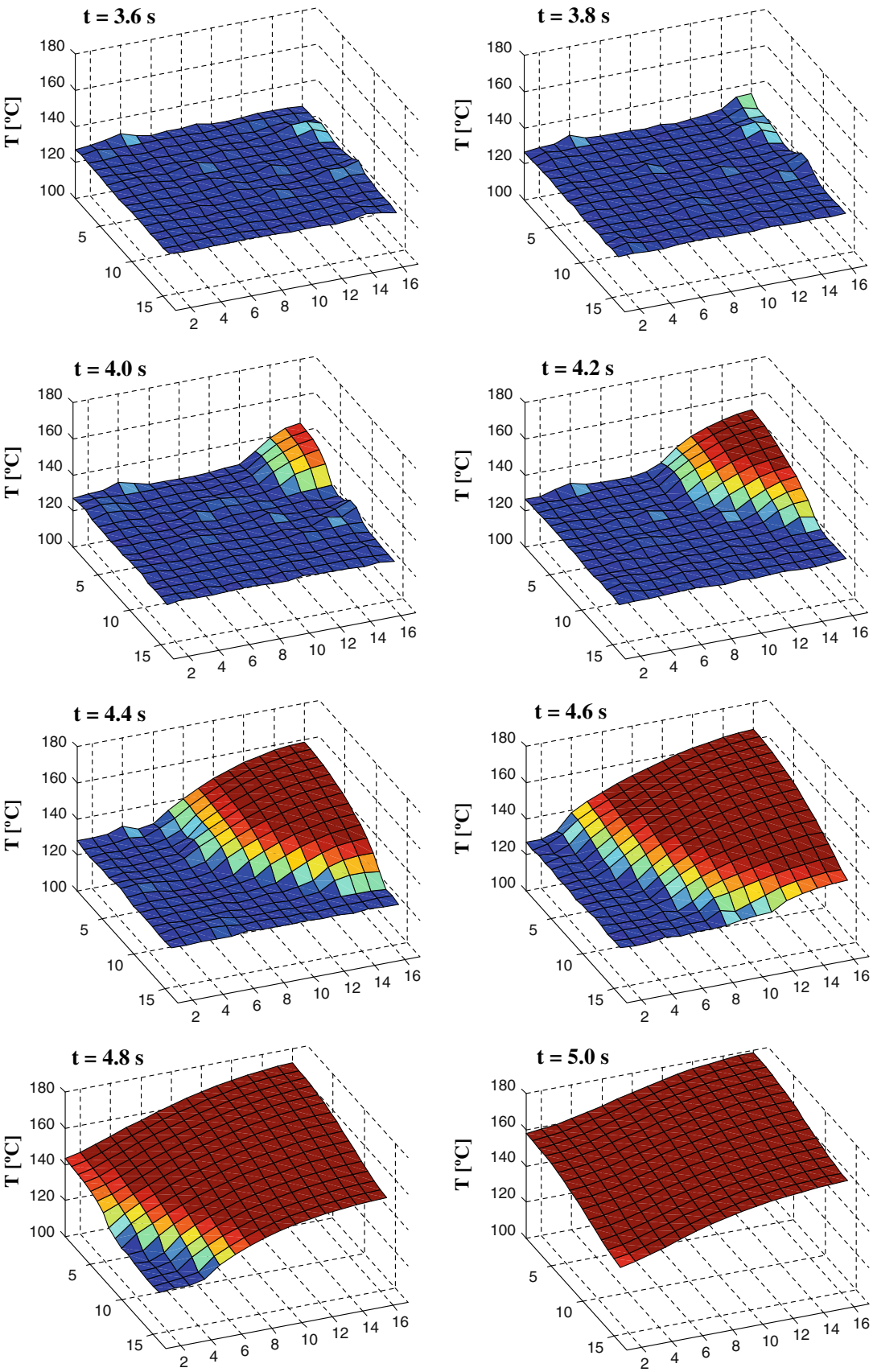

Fig. 11 Temporal evolution of the heater temperature in a case in which CHF was reached

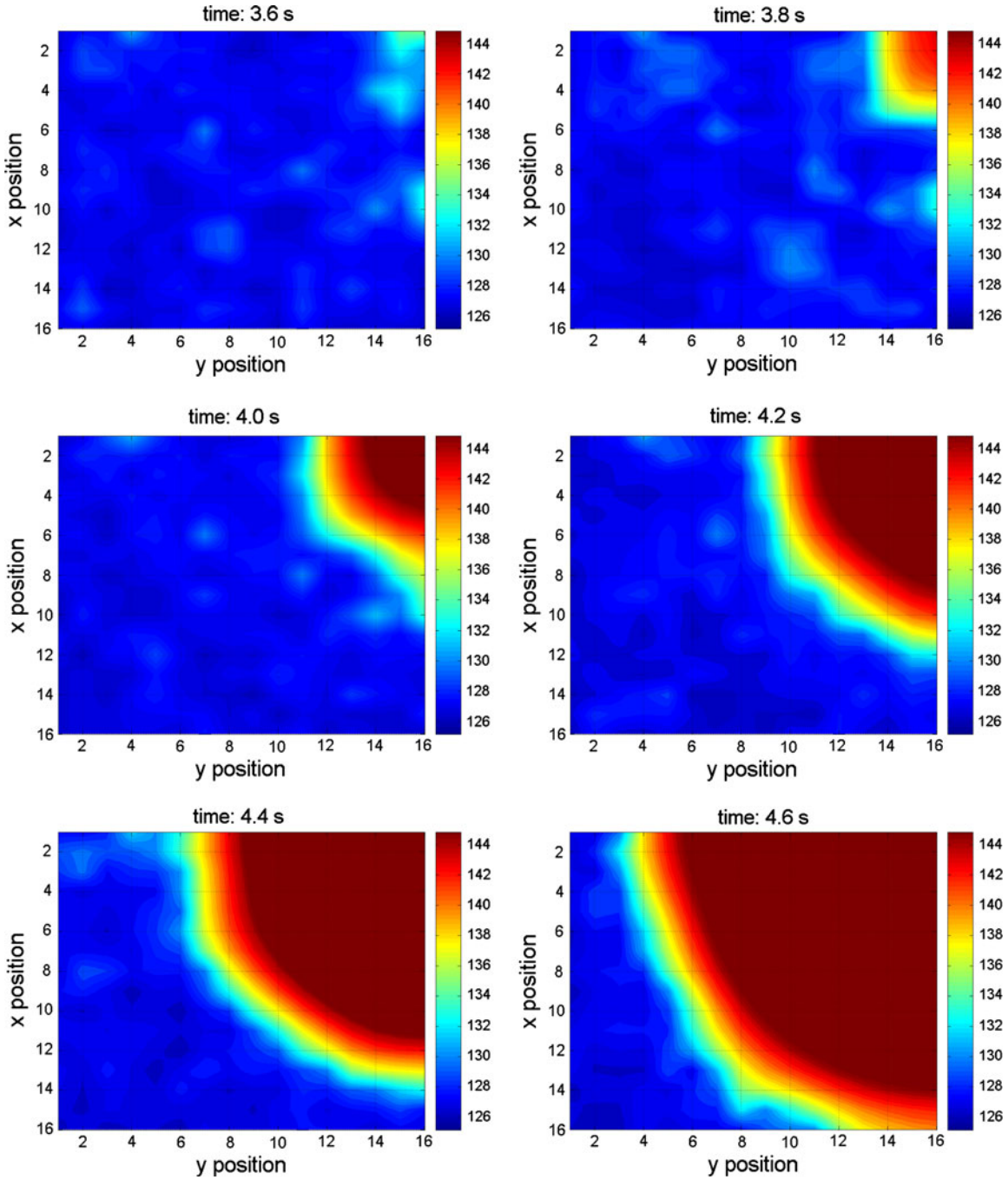

Fig. 12 Temporal evolution of the distribution of the heater temperature

The surface-blanketing characteristic of the film-boiling regime is simulated by the insulation of the fractions of surface intersected by bubbles (which occurs at high heat fluxes when large bubbles are formed by coalescence above the heater). The automata simulations predict that for power levels higher than a certain threshold, the heater cell temperatures escalate rapidly as a consequence of the boiling crisis. Figure 11 depicts the temporal evolution of the heater temperature, showing the sudden escalation associated with the CHF. The power level in this case is 145 W/cm^2. A remarkable characteristic of the CHF simulated by the pool boiling automata is propagation velocity of the temperature escalation through the heater surface. In order to better understand this phenomenon, 2D contour plots of selected frames of this process are depicted in Fig. 12. These frames represent a short sequence of 1 s.

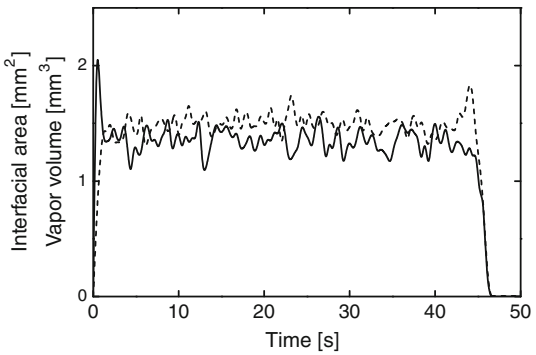

Fig. 13 Temporal evolution of the interfacial area and the vapor volume in proximities of the heater (123 W/cm^2)

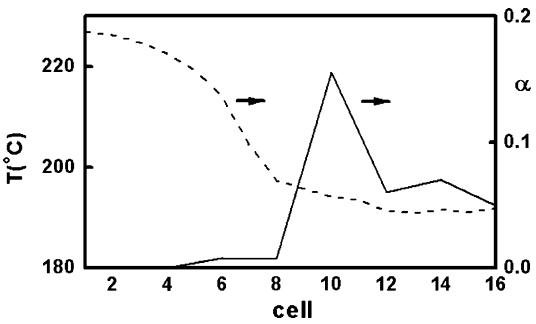

Fig. 14 Void fraction (*solid*) and wall temperature (*dash*) profiles. The *arrows* indicate the direction of the movement of the CHF front

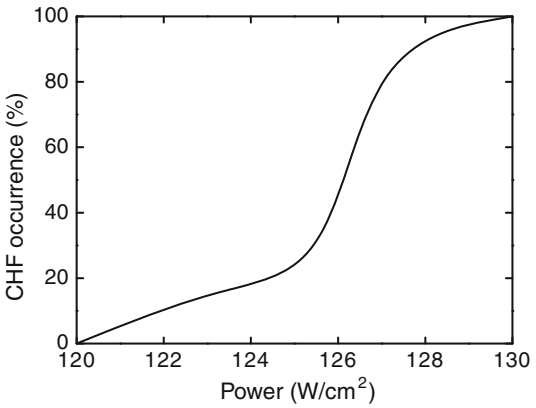

Fig. 15 CHF statistics of the pool boiling automata

The color represents the heater superheat. At 3.6 s, no hot spots are observed and low temperature prevails in most of the area due to the ongoing nucleation and vapor generation. In the subsequent frames, the temperature starts to increase at one corner. At 4.4 s, the temperature escalation covers about 45% of the heater. The propagation lasts no more than 1 s resembling a domino effect. Once a vapor blanket isolates a cell, the cell power can no longer be extracted through the cell surface (radiation as heat transfer mechanism requires much higher surface temperatures in order to dissipate all the cell power), and therefore the heat

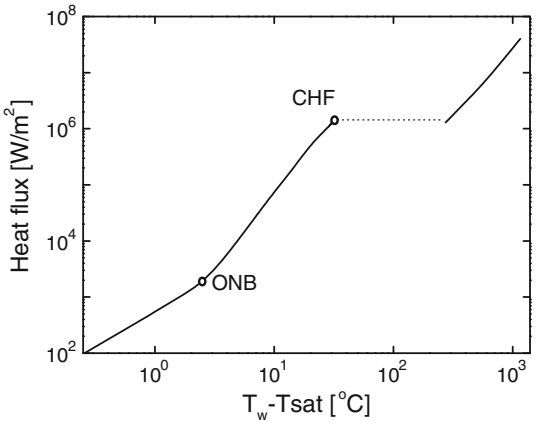

Fig. 16 Boiling curve predicted by the automata model for water at 1 atm

flux streams out to the neighbor cells by conduction. Adjacent cells then transfer more heat to the liquid, which rapidly generates more vapor near their surface, producing in turn their own blanketing, and so on. This result agrees with experiments reported in literature where notable similar evolutions of the blanketing front were observed [50]. A curious characteristic is that the CHF events of the automata generally start in border cells, which was also observed in real experiments [50]. This is reasonable since the peripheral cells have less neighbor cells to help them to extract the heat when occasional vapor blanketing occurs.

In order to study the topology of the two phase flow right before the onset of CHF, the evolution of the interfacial area and volume were calculated in a 5-mm thick control volume placed above the heater dissipating 123 W/cm^2. The result is shown in Fig. 13. As can bee seen, at the beginning the interfacial area grows rapidly according to the increase number of bubbles. Interestingly the largest value of the interfacial area does not correspond to the maximum amount of vapor in the system. Initially there are most of the bubbles sizes correspond to the detaching radii. As the bubble population grows, coalescence increases, and consequently the value of the interfacial area decreases. After this initial behavior, the two variables reach a certain steady state until the CHF mechanism is triggered, which can be seen in Fig. 13 at $\sim$44 s, when the interfacial area suddenly decreases in the control volume while the vapor volume remains unchanged, indicating a change in the topology of the two phase flow in the vicinity of the heater. This result agrees with the Kutateladze theory that attributes the initiation of the boiling crisis to a drastic transition in the flow topology [22]. After the CHF development all the sites stop producing vapor and therefore the interfacial area and the vapor volume drop to zero. Actually, vapor is produced at the film interface, but this mechanism was not modeled here. Figure 14 shows the instantaneous void fraction and wall temperature profiles along the heater center line. It can

be seen how the void fraction wave-front precedes the burnout wave. Remarkably, a similar wave was recently observed experimentally by Buchholz et al. [50].

It is well known that the CHF is a statistical phenomenon. The boiling crisis does not occur always at the same time even with experiments at the same power, regardless of how well the experimental parameters are controlled. In order to study the statistics of CHF, many numerical calculations were performed with the boiling automata for each power level using different random number generator seeds. If during 60 s there was no temperature escalation, a negative case was counted. Figure 15 shows the occurrence of CHF at different power levels. It can be seen that for power levels higher than 130 W/cm^2, CHF always occurs, which is in agreement with the experimental data of pool boiling in water with small heaters. The sensitivity coefficient of this result to the grid resolution is 0.008, which ensure the robustness of the model.

In addition to the results presented above, the automata model was used to predict the boiling curve [16]. The result of this simulation is shown in Fig. 16. As can be seen, most of the characteristics of the Nukiyama curve are well reproduced. The free convection regime and the nucleate boiling regime agree well with reported values found in literature [51]. It is worth mentioning that experimental value of CHF in water is predicted by model surprisingly well which corroborates the capability of the formulation presented in this work. The film boiling regime is somehow located at lower temperatures than in the experiments. This part of the curve, however, is largely affected by the surface emissivity of the heating surface which in turn depends on the heater surface.

7 Conclusions

A novel automata model of boiling phenomena was presented. The main difference of the present approach respect to other automata models [12, 52] is that the bubbles move and interact in continuous space, involving not only evaporation and rising but also coalescence and breakup.

Numerical experiments showed that the algorithms can capture the essential features underlying the boiling phenomena around small heaters, such as boiling heat transfer, bubble formation, boiling crisis, and the interactions with the heater surface. The results presented in this work should be seen from a perspective of the potential of the new approach to treat the complicated phenomena involved in boiling systems. It is hoped that this study stimulate further investigations of two-phase systems using statistical inspired theories.

Among many interesting topics for further developments of bubble automata theory, the most important are the formulation of a more general theoretical framework towards a geometric statistics, and applications to experimental techniques. It is our hope that the method presented in this paper will encourage other researchers in the field of boiling heat transfer to explore the great potential offered by computer automata. By means of this attempt, without invalidating the important advances obtained in other directions, a new tool is offered whose exploitation is greatly exceeded by its potential.

References

1. Wallis G (1969) One-dimensional two-phase flow, chap 2. McGraw-Hill, New York
2. Zuber N, Findlay J (1965) Average volumetric concentration in two-phase systems. J Heat Transf 87:453–468
3. Cooper N (ed) (1987) Los Alamos science special issue. Los Alamos National Laboratory, New Mexico
4. Ulam S (1958) John von Neumann, 1903–1957. Bull Am Math Soc 64:1–49
5. Wolfram S (1986) Cellular automata fluids. J Stat Phys 45:3–4
6. Herault A, Vicari A, Ciraudo A, Del Negro C (2008) Forecasting lava flow hazards during the 2006 Etna eruption: using the MAGFLOW cellular automata model. Comput Geosci (in press)
7. Fan Y, Ying S, Wang B, Wei Y (2008) The effect of investor psychology on the complexity of stock market: an analysis based on cellular automaton model computers and industrial engineering (in press)
8. Slimi R, El Yacoubi S, Dumonteil E, Gourbière S (2008) A cellular automata model for Chagas disease. Appl Math Model (in press)
9. Shoham Y (1993) Agent-oriented programming. Artif Intell 60:51–92
10. Meyer B (1997) Object-oriented software construction, 2nd edn. Prentice-Hall, Englewood Cliffs
11. Herrero V, Guido-Lavalle G, Clausse A (1996) Geometrical automata for two phase flow simulation. Nucl Eng Des 163:117–124
12. Jing Y, Guo L, Zhang X (2003) A numerical simulation of pool boiling using CAS model. Int J Heat Mass Transf 46:4789–4797
13. Chen T, Chung JN (2002) Coalescence of bubbles in nucleate boiling on microheaters. Int J Heat Mass Transf 45:2329–2341
14. Booch G (1991) Object oriented with applications. Benjamin/Cummings Publishing Company, Inc., Redwood City
15. Leidenfrost JG (1966) De aquae communis nonnullis qualitatibus tractatus (A tract about some qualities of common water), Duisburg, 1756; The pertinent portions are reprinted in translation in Int J Heat Mass Transf 9:1153
16. Nukiyama S (1966) The maximum and minimum values of heat transmitted from metal to boiling water under atmospheric pressure. Int J Heat Mass Transf 9:1419
17. Forster HK, Zuber N (1955) Dynamics of vapor bubbles and boiling heat transfer. AIChE J 1(4):531–535
18. Forster KE, Greif R (1959) Heat transfer to a boiling liquid mechanism and correlations. J Heat Transf 81:43–53
19. Han CY, Griffith P (1965) The mechanism of heat transfer in nucleate pool boiling. Int J Heat Mass Transf 8:887–914
20. Mikic BB, Rohsenow WM (1969) A new correlation of pool boiling data including the effect of heating surface characteristics. J Heat Transf Trans ASME 91:245–250
21. Snyder NW (1956) Summary of conference on bubble dynamics and boiling heat transfer, JPL memo 20-137, Jet Propulsion laboratory, California Institute of Technology

22. Kutateladze SS, Leont'ev AI (1966) Some applications of the asymptotic theory of the turbulent boundary layer. In: Proceedings of the 3rd international heat transfer conference, New York
23. Thorgeson EJ, Knoebel DH, Gibbons JH (1974) A model to predict convective subcooled critical heat flux. J Heat Transf 96:79–82
24. Katto Y, Yokoya S (1968) Principal mechanism of boiling crisis in pool boiling. Int J Heat Mass Transf 11:993–1002
25. Matorin AS (1973) Correlation of experimental data on heat transfer crisis in pool boiling of pure liquids and binary mixtures. Heat Transfer Sov Res 5:85
26. Costello CP, Book CO, Nichols CN (1963) A study of induced convective effects on saturated pool boiling burnout. Chem Eng Prog Symp Ser 61:271
27. Tong LS (1972) Boiling crisis and critical heat flux. AEC Critical Review Series, USAEC
28. Whalley PB, Hutchinson P, Hewitt GF (1974) Calculation of critical heat flux in forced convection boiling. In: 5th International heat transfer conference, Tokyo
29. Lahey R Jr (ed) (1992) Boiling phenomena. Elsevier, Amsterdam, pp 86–91
30. Carrica P, Clausse A (1994) A mathematical model of local boiling nonlinear dynamics and crisis. Lat Am J Appl Res 24:77–83
31. Van Stralen S, Cole R (1979) Boiling phenomena, vol 1. McGraw-Hill, NY, 130 pp
32. Cooper M (1970) The microlayer and bubble growth in nucleate pool boiling. Int J Heat Mass Transf 13:656–666
33. Cooper M, Lloyd J (1970) Transient local heat flux in nucleate boiling. In: Proceedings of the 3rd international heat transfer conference, Chicago, vol 3, B2.1. Elsevier, Amsterdam
34. Cooper M, Lloyd J (1969) The microlayer in nucleate pool boiling. Int J Heat Mass Transf 12:895–913
35. Cooper M, Vijuk R (1970) Bubble growth in nucleate pool boiling. In: Proceedings of the 4th international heat transfer conference, Paris, Versailles, vol 5, B2.1. Elsevier, Amsterdam
36. Fritz W (1935) Berechnung des Maximalvolumens von Dampfblasen. Physics 36:379–384
37. McAdams W (1954) Heat transmission, chap 4, 3rd edn. McGraw-Hill, New York
38. Goldstein R, Sparrow E, Jones D (1973) Natural convection mass transfer adjacent to horizontal plates. Int J Heat Mass Transf 16:1025–1030
39. Lloyd J, Moran W (1974) Natural convection mass transfer adjacent to horizontal surfaces of various platforms. ASME, 4-WA/HT-66
40. Van Stralen S, Cole R (1979) Boiling phenomena, vol 2. McGraw-Hill, New York, pp 456–458
41. Lahey R Jr (ed) (1992) Boiling phenomena. Elsevier, Amsterdam, pp 402–404
42. Incropera F, Dewitt D (2006) Fundamentals of heat and mass transfer, 5th edn. Wiley, New York
43. Stephan P, Fuchs T (2009) Local heat flow and temperature fluctuations in wall and fluid in nucleate boiling systems. Heat Mass Transf 45:919–928
44. Golobic I, Petkovsek J, Baselj M, Papez A, Kenning DBR (2009) Experimental determination of transient wall temperature distributions close to growing vapor bubbles. Heat Mass Transf 45:857–866
45. Chen T, Chung JN (2002) Coalescence of bubbles in nucleate boiling on microheaters. Int J Heat Mass Transf 45:2329–2341
46. Marcel CP, Rohde M, Van der Hagen THJJ (2008) Fluid-to-fluid modeling of natural circulation boiling loops for stability analysis. Int J Heat Mass Transf 51:566–575
47. Serizawa A, Kataoka I, Michiyoshi I (1975) Turbulence structure of air–water bubbly flow—II. Local properties. Int J Multiph Flow 2:235–246
48. Žun I (1980) The transverse migration of bubbles influenced by walls in vertical bubbly flow. Int J Multiph Flow 6:583–588
49. Wang SK, Lee SJ, Jones OC Jr, Lathey RT Jr (1987) 3-D turbulence structure and phase distribution measurements in bubbly two phase flows. Int J Multiph Flow 13:327–343
50. Buchholz M, Lüttich T, Auracher H, Marquardt W (2004) Experimental investigation of local processes in pool boiling along the entire boiling curve. Int J Heat Fluid Flow 25:243–261
51. Van Stralen S, Cole R (1979) Boiling phenomena, vol 2. McGraw-Hill, New York, 632 pp
52. Gupta A, Ghoshdastidar P (2006) A three-dimensional numerical modeling of atmospheric pool boiling by the coupled map lattice method. ASME J Heat Transf 128:1149–1158